Original Article

Bei Ma, Pan Liu, Yaofeng Zhang, Lijun Tang, Zhengyang Zhao, Ze Ding, Tianyang Wang, Tianzhen Dong, Hongwei Chen* and Junfeng Liu*

Hydrogel for slow-release drug delivery in wound treatment

https://doi.org/10.1515/polyeng-2024-0094 Received May 28, 2024; accepted July 30, 2024; published online August 23, 2024

Abstract: When skin comes into direct contact with the outside environment, it becomes extremely prone to injury and external factors can make wounds difficult to heal. Traditional medical dressings often cause secondary injury and are poorly resistant to infection. Hydrogels offer a promising alternative to overcome these difficulties. In this study, chitosan (CS)/gelatin (GEL)/polyvinyl alcohol (PVA) hydrogels were developed by chemical cross-linking and loaded with the drug kitasamycin (KM) for testing. The hydrogels' in vitro drug release and wound-healing properties were assessed. For 48 h, the drug release from the hydrogel in vitro persisted, which was significantly longer than the release time of the KM solution. Antimicrobial activity tests showed that the loaded KM hydrogel maintained its bacteriostatic ability at the same concentration as the KM solution, and during in vitro bacteriostatic inhibition, the duration of bacteriostatic inhibition of the KM hydrogel was significantly prolonged compared to that of the KM solution. This confirms the controlled release capability of the hydrogel. In addition, the hydrogel reduced the wound size in mice by 96 % and histopathological tests showed complete re-epithelialization of the wound. The prepared

Bei Ma and Pan Liu contributed equally.

*Corresponding authors: Hongwei Chen and Junfeng Liu, College of Animal Science and Technology, Tarim University, Alar 843300, Xinjiang, P.R. China; and Engineering Laboratory of Tarim Animal Diseases Diagnosis and Control, Xinjiang Production & Construction Groups, Alar 843300, Xinjiang, P.R. China, E-mail: chwdky@126.com (H. Chen), ljfdky@126.com (J. Liu)

Bei Ma, Pan Liu, Yaofeng Zhang, Zhengyang Zhao, Ze Ding, Tianyang Wang and Tianzhen Dong, College of Animal Science and Technology, Tarim University, Alar 843300, Xinjiang, P.R. China; and Engineering Laboratory of Tarim Animal Diseases Diagnosis and Control, Xinjiang Production & Construction Groups, Alar 843300, Xinjiang, P.R. China Lijun Tang, College of Animal Science and Technology, Tarim University, Alar 843300, Xinjiang, P.R. China; and Si Chuan Vocational and Technical College, Suining 629000, Si Chuan, P.R. China

hydrogels successfully demonstrated their potential ability to control drug release and promote skin wound healing.

Keywords: hydrogel(s); drug delivery system; controlled drug release; antimicrobial; wound healing

1 Introduction

The largest organ in the human body, the skin, serves a number of purposes, including as controlling body temperature, detecting environmental cues, and shielding the body from harm. However, due to the skin's direct exposure to the outside world, it is highly susceptible to injury, and the healing process is accompanied by the presence of external pathogens and inflammatory factors that interfere with the repair process. To address this problem, good moisturizing properties of wound dressings to maintain a moist wound environment, low irritation, and excellent biocompatibility² play a crucial role in providing a temporary barrier to external factors³ and creating an optimal environment for wound healing.4 Hydrogel dressings are a class of highly hydrophilic gels with a three-dimensional network structure⁵ that can absorb wound exudate without adhering to the wound. This means that dressing changes do not cause additional damage to the granulation or epithelial tissue. ⁶ In addition, hydrogel dressings maintain a moist environment and facilitate the enzymatic breakdown of necrotic tissue, creating an optimal healing environment that exceeds that of conventional medical dressings.

The undisputed advantages of hydrogel preparation and application include its rapid gelation, no need for cross-linking agents, self-healing, and injectable properties. The present experimental hydrogel preparation method (Figure 1) is simple and nontoxic to prepare by using Schiff base reaction in conjugation reaction in chemical cross-linking. The biological effects of Schiff bases have also been shown to be extensive, containing anti-inflammatory, antibacterial, antiproliferative, and antipyretic properties. In contrast to other dynamic links found during the hydrogel preparation process, the Schiff base reaction is fast and can

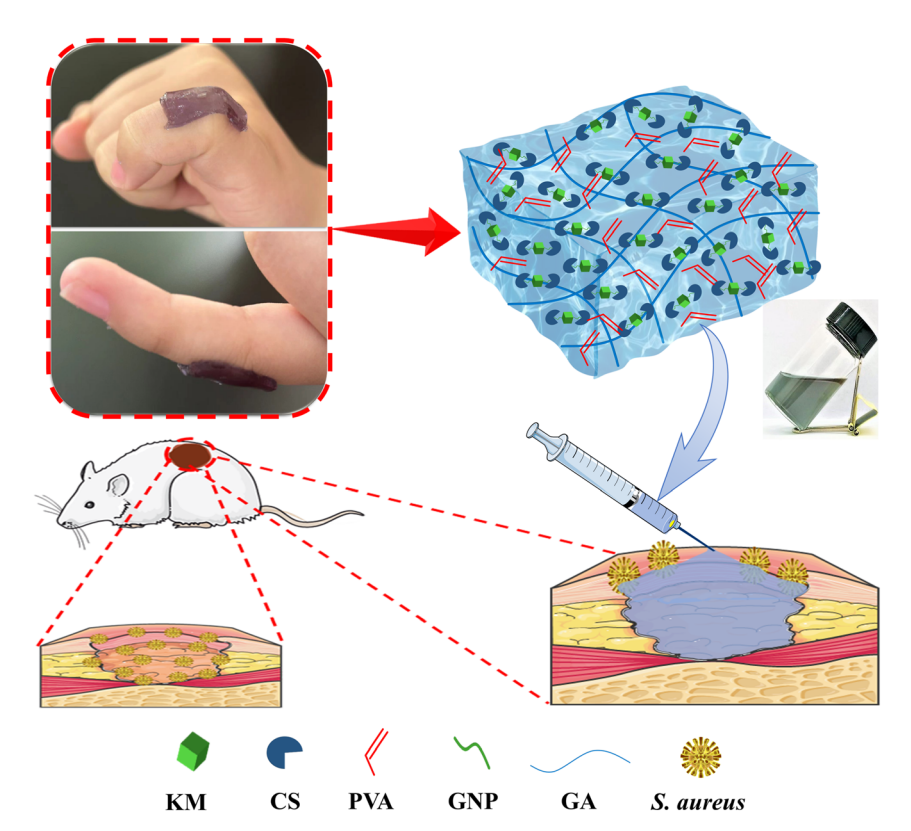


Figure 1: Preparation and application of KM hydrogels.

be easily carried out under mild conditions without the need for other reaction conditions such as catalysts.

The test drug KM was chosen in this paper because Staphylococcus (S.) aureus is still the causative organism most likely to cause serious infections in the clinic, and the drugs used to treat Staphylococcus aureus infections in the clinic mainly focus on sulfonamides and antibiotics, ⁹ but its resistance to commonly used antibiotics such as penicillin G, erythromycin, and tetracycline is increasing every year and has already become a major problem in clinical treatment. KM is a low-toxicity macrolide antibiotic produced by Streptomyces, which is widely used for upper respiratory tract infections, pneumonia, and skin and soft tissue infections caused by Gram-positive bacteria and mycoplasma.¹⁰ Chen Taiding et al.¹¹ showed that the inhibition rate of KM against Aureobasidium was 59.7%, which was significantly better than that of erythromycin (35.8%) and penicillin G (40 %). However, due to the poor water solubility of KM currently used in clinical practice, the blood concentration is lower than that of other macrolide antibiotics, ¹² so it is necessary to administer the drug in sufficient amounts and frequently to achieve the therapeutic purpose. Therefore, in this study, we applied the high drug loading rate and high stability of the hydrogel, which can be actively targeted by attaching ligands that recognize homologous receptors on target cells or tissues to achieve controlled

release, to improve the shortcomings of KM in current clinical application, for the purpose of enhancing the clinical KM's therapeutic effect.

2 Materials and methods

2.1 Materials

Kitasamycin solution (KM, CAS: 1392-21-8) and polyvinyl alcohol (PVA, CAS: 9002-89-5) were purchased from Shanghai McLean Biochemistry Science and Technology Co. Ltd (China); chitosan (CS, CAS: 9012-76-4) and genipin (GNP, CAS: 6902-77-8) were purchased from Beijing Solepco (China); gelatin (GEL, CAS: 9000-70-8) was purchased from Sinopharm Chemical Reagent Co. Tumor necrosis factor- α (TNF- α) antibody, interleukin-1 β (IL-1 β) antibody, platelet endothelial cell adhesion molecule (CD31) antibody, monocyte-macrophage molecule (CD68) antibody were provided by China Said Biotechnology Co.

S. aureus ATCC29213 and small colony variant *aureus* (SCVA) were provided by the Tarim Animal Disease Diagnosis, Prevention and Control Engineering Laboratory of the Xinjiang Production and Construction Groups.

Kunming mice (18-22 g) and New Zealand rabbits (2–2.5 kg) were provided by Viton Lever Laboratory Animal Technology Ltd (China). Animal experiments were performed in accordance with the National Institutes of Health's Guide for the Care and Use of Laboratory Animals (NIH Publication No. 8023, Revised 1978).

2.2 Preparation of CS/GEL/PVA hydrogels

The KM solution was slowly dripped into chitosan and stirred at 1,500 rpm, 50 °C for 1h in a WH240-HT digital constant temperature magnetic stirrer (purchased from Suzhou (China) Sainz Instruments Co, Ltd) for drug encapsulation. The encapsulated material was slowly dropped into PVA aqueous solution at 1,500 r/min, 50 °C for 1 h for chemical cross-linking to form KM-loaded CS/PVA hydrogels; slowly drop GNP into the loaded CS/PVA hydrogel and CS at 1,500 rpm, 50 °C stirred for 1 h to occur Schiff base reaction to increase its stability and cross-linking; after cross-linking to form a stable loaded KM hydrogel to add GEL to increase its mechanical strength and swelling properties. The KM-loaded hydrogel was placed in the refrigerator at 4 °C to remove air bubbles, and then the color changed to blue.

2.3 Hydrogel drug loading assay

2.3.1 Determination of drug absorption wavelength

Weigh 0.1 g of KM accurately and add it to 95 % anhydrous ethanol to make 0.1 % KM standard solution (I) and 0.001 % KM standard solution (II).KM standard solution (I) and 0.001% KM standard solution (II). Scanning was carried out on a UV-1900i UV spectrophotometer (purchased from Shimadzu Science and Technology Co., Ltd., Japan).

2.3.2 Establishment of drug standard curve

KM was accurately weighed and serially diluted into different concentrations (16, 8, 4, 2, 1, and 0.5 µg/mL) of KM solution with deionized water and then passed through a 0.22 µm microtiter filter, and its OD value was determined using a UV spectrophotometer at the wavelength of maximum absorption (228 nm) and its standard curve was plotted.

2.3.3 Hydrogel encapsulation rate and drug loading assay

Determine the hydrogel encapsulation rate (EE) and drug loading capacity (LC) based on 2.3.2. The prepared drugloaded hydrogel was centrifuged at 14,000 rpm for 60 min at 4°C, and the supernatant and sinker were collected. The supernatant was filtered, and then the free KM content was measured by a UV spectrophotometer to calculate the EE. The hydrogel-encapsulated KM in the sinker was measured by the JY92-IIN Cell Breaking Ultrasonic Instrument (purchased from Jinan (China) Ouleb Scientific Instrument Co., Ltd). Then, the supernatant after centrifugation at 8,000 rpm for 10 min was measured by UV spectrophotometer to determine the content of KM to calculate the LC.

$$EE = (M/MKM) \times 100 \%$$
 (1)

$$LC = (M/MGEL) \times 100 \%$$
 (2)

where MKM is the total amount of KM, /g, M is the amount of KM in the hydrogel, /g, and MGEL is the total amount of hydrogel, /g.

2.4 Evaluation of hydrogel characterization

2.4.1 Swelling property test

The hydrogel swelling kinetics was tested by the mass method as follows: the freeze-dried hydrogel samples were immersed in pH 7.4 and pH 5.5 phosphate buffered saline (PBS) using an EYELA freeze dryer (FDU-1200 Tokyo Riken). The samples were taken out every 2 h, and the mass was weighed after wiping off the water from the surface of the samples with filter paper and recorded.

$$WS = (Wt - W0)/W0 \times 100 \%$$
 (3)

where WS is the swelling rate, Wt is the mass of hydrogel after swelling, /m, and W0 is the mass of hydrogel after lyophilization, /m.

2.4.2 Particle size and zeta potential

The loaded KM hydrogel, diluted 100 times with deionized water, was sonicated for 30 min and placed in a quartz cuvette, and the particle size and zeta potential of the KM hydrogel were determined using a Malvern Nano-ZS90 Nano Particle Size and Zeta Potential Analyzer (Spectrum Instrument Systems Co., Ltd, Shanghai, China).

2.4.3 Scanning electron microscopy (SEM)

Freeze-dried gel samples were taken and stuck to the SEM sample discs with conductive adhesive, sputtered and sprayed with gold, and then used an SU8700 scanning electron microscope [Hitachi Scientific Instruments (Beijing) Co.].

2.4.4 Fourier transform infrared spectroscopy (FT-IR)

The freeze-dried KM hydrogel was ground to powder, mixed with potassium bromide 1:100, and pressed into a transparent sheet form, and specific peaks in the 4,000–500 cm⁻¹ wavelength range were determined using a NEXUS 470 model Fourier Transform Infrared (FT-IR) spectrometer (Rigaku, Japan).

2.4.5 X-ray diffraction (XRD)

The crystalline structure of KM hydrogels was investigated using a Rigaku Smart Lab SE X-ray diffractometer (Nicolet, USA). The test conditions were copper target, tube current 40 mA, tube voltage 40 kV, scan speed 2°/min, and diffraction angle 5°-50°.

2.5 Hydrogel in vitro release rate assay

Take 200 mL of PBS (pH 7.4 vs. pH 5.5) and put it into a 37 °C intelligent thermostatic culture shaker to preheat and set aside. Aspirate 2 mL of KM hydrogel and 2 mL of KM solution of the same concentration into the treated dialysis bag, put the dialysis bag into a beaker containing PBS of pH 5.5 and pH 7.4, respectively, and perform the release test at a constant rate. Every 2h, 2mL was aspirated (each time after the removal of the bag, it was necessary to replenish into the same volume of PBS buffer with the same pH), the OD value was measured and brought into the standard curve to calculate the content of kitasamycin, the time was used as the horizontal coordinate, and cumulative release percentage was used as the vertical coordinate of plotting.

2.6 Antibacterial activity of hydrogel

2.6.1 Determination of minimum inhibitory concentration

The micro broth dilution method was used to determine the minimum inhibitory concentration (MIC) of KM APIs with loaded KM hydrogels. Gradient dilution of the drug to be tested was carried out with MH broth medium, to which 1×10^6 CFU/mL of S. aureus ATCC29213 with SCVA was added, and then the above drug-containing bacterial liquid was added in a sterile 96-well plate, after which positive and negative controls were set. The plates were incubated overnight at 37 °C in a constant temperature incubator, and the turbidity of the liquid in the well plates was compared,

where the lowest concentration of the drug in the wells with clear liquid was taken as the MIC of the drug.

2.6.2 Detection of bacterial inhibition by agar perforation method

Add 200 uL of 1×10^8 CFU/mL log phase bacterial solution to the MH agar medium plate and spread it evenly with a coating stick; punch 4 holes on the MH agar medium coated with bacterial solution; and dilute 3 concentrations of KM aqueous gel (1 %, 0.10 %, 0.01 %) at high, medium, and low concentrations as test samples and add 50 µL of samples to each hole, while using sterilized deionized water as negative control and the same concentration of KM solution and blank gel auxiliaries as positive control. The same concentration of KM solution and blank gel auxiliaries were used as the positive control and placed in a 37 °C constant temperature incubator, and the inhibition circle was measured after overnight, and the size of the inhibition circle was compared.

2.6.3 In vitro bacterial inhibition curve plotting

The 1×10^6 CFU/mL log phase test bacterial solution was mixed with KM hydrogel and KM solution to its concentration of 1/2 MIC, MIC containing bacterial solution, respectively, and the other drug-free containing bacterial broth medium was used as positive control. The number of bacteria was detected by Micro Screen-HT high-throughput real-time microbial growth meter (Tianjin (China) Jieling Instrument Manufacturing Co., Ltd), and the bacterial inhibition curves of 1/2 MIC and MIC drug concentrations on the test bacterial solutions were plotted with the number of bacteria as the vertical coordinate and the time point as the horizontal coordinate.

2.7 Hydrogel safety studies

2.7.1 Blood compatibility test

Healthy New Zealand rabbits (male, 3 months old, 2.0–2.5 kg, healthy) were given 5 mL of fresh blood from the earlobe vein, centrifuged at 2,000 rpm for 5 min at room temperature, the red blood cells in the bottom layer were collected, the red blood cells were washed repeatedly with PBS for 3 times, and the red blood cells were configured into a 5 % red blood cell suspension with PBS and dispensed into centrifuge tubes, 1 mL of red blood cell suspension in each tube, and the supernatant was discarded after centrifugation; the KM hydrogel was graded and diluted with PBS to 1 mg/mL,

0.1 mg/mL, 0.01 mg/mL; add 1 mL of the diluted loaded KM hydrogel solution to the EP tubes of the experimental group, 1 mL of deionized water for the positive control group, 1 mL of PBS solution for the negative control group, and blow gently to mix well; place the EP tubes in the 37 °C thermostat and incubate for 12 h. Observe the color of the solution after centrifugation, and take 100 uL of the supernatant was tested for absorbance at 450 nm with an enzyme meter.

$$Hs = (Ht - Hb)/(Hc - Hb) \times 100 \%$$
 (4)

where Hs is the hemolysis rate, Ht is the experimental group, Hb is the negative control group, and Hc is the positive control group.

2.7.2 Cytotoxicity test

The cytotoxicity test of the KM hydrogel was performed using the CCK-8 kit. The cell suspension was inoculated into 96-well plates after adjusting the density of dairy cow mammary epithelial cells (MAC-T) to 1×10^3 cells/mL using a cell counter. The well plates were placed in a cell culture incubator (37 °C, 5 % CO₂) for 12 h to allow the cells to attach to the wall, and then the liquid was changed. KM hydrogel with 0.22 µm microporous filter was used for filtration and sterilization, and the media solution with DMEM complete medium containing 10 % fetal bovine serum and 1 % double antibody was gradient-diluted to 1 mg/mL, 0.1 mg/mL, and 0.01 mg/mL of KM hydrogel and coincubated with the cells. When MAC-T cells and QC-4 were coincubated for 24 h, 48 h, and 72 h at different time points, the well plates were removed, the medium in the empty plates was discarded, 100 μL of serum-free basal medium was added, and 10 μL of CCK-8 reagent was added to each well. The plates were incubated in a cell culture incubator for 2 h, then removed, and the absorbance OD value at 450 nm was read under the HBS-1096 A enzyme labeling instrument (Nanjing (China) DeTie Experimental Equipment Co.). The cell proliferation rate was calculated as follows:

Cell proliferation rate% =
$$(ODt - ODb)/(ODp - ODb)$$

 $\times 100 \%$ (5)

where the OD value of blank group (complete medium + CCK-8) was recorded as ODb, control group (cells + complete medium + CCK-8) was recorded as ODp, and experimental group (cells + QC-4 + complete medium + CCK-8) was recorded as ODt.

2.7.3 Cell migration experiment

MAC-T cells at a density of approximately 90 % were crossed with a 10 µL tip against a ruler, with each cross line spaced 0.5-0.8 cm apart, and three cross lines were passed through each well. The cells under the cross lines were washed three times with PBS. Then, 1.5 mL of DMEM low serum medium containing 1 mg/mL, 0.1 mg/mL, and 0.01 mg/mL of KM hydrogel was added to the well plates, and the cells were cultured in a cell culture incubator at 37 °C with 5 % CO₂. After that KM hydrogel and MAC-T cells were incubated. The well plates were removed at 0 h, 6 h, 12 h, and 18 h and placed under an inverted microscope for observation.

2.8 Assessment of body wound healing

Selected Kunming lineage mice were purchased from the College of Animal Science and Technology, Tarim University, and placed in the animal house after 1 week of guarantine with normal feed and water supply. All mice were divided into three groups, namely control group (saline only), KM API group, and KM hydrogel group and kept in differently labeled cages for identification. The rats were anesthetized using ketamine hydrochloride 60 mg/mL), and the hair on the back was removed, after which the skin was cleaned with a cotton swab and a wound of 1.5 cm in diameter was established on the back of the mice. Then, a section of prepared hydrogel was placed on the wound of each mouse in the KM hydrogel group. The size of each wound was recorded using a digital Vernier caliper, and the healing rate was estimated on days 0, 3, 7, and 14 by the following equation.

Healing rate formula:
$$(S0 - St)/S0 \times 100 \%$$
 (6)

where S0 denotes the original wound size on day 0, and St denotes the wound size on days 3, 7, and 14.

2.9 Histopathological examination

Traumatized skin from isolated mice, together with adjacent normal skin, was collected, fixed, paraffin-embedded, and sectioned (4-6 µm thick). The tissue sections were then stained with hematoxylin and eosin (H&E), Masson, immunohistochemistry (IHC), and immunofluorescence (IF) to assess epidermal regeneration. The prepared slides were visualized under a section scanner. To compare the results, one-way ANOVA and post hoc Tukey tests were used for statistical evaluation, with a "p" value of less than 0.05 for Graphpad prism 5. Results are expressed as the mean ± SD of each analysis.

3 Results and discussion

3.1 Hydrogel drug loading assay

3.1.1 Maximum absorption wavelength determination

Figure 2A shows that KM has a maximum absorption peak of Kmax = 228 nm in the UV-visible region, which is basically equal to the absorbance measurement value (231 nm) of the KM standard of the 2020 edition of the Chinese Pharmacopoeia, Part II, after removing the interfering factor. Therefore, it can be determined that the purchased drug is the standard, and the experimental results are reliable.

3.1.2 Drug standard curve establishment

The standard curve was plotted with the drug concentration as the horizontal coordinate and the OD value as the vertical

coordinate (Figure 2B). The linear regression equation was y = 0.0313x - 0.0071 ($R^2 = 0.9997$), and the results showed that the KM had an excellent linear relationship with the OD value in the concentration range of 0.5–16 mg/mL.

3.1.3 Hydrogel encapsulation rate and drug loading detection

The results of the orthogonal test by selecting four factors that have a greater influence on the hydrogel are shown in (Table 1); from the table, it can be seen that when the more CS the higher the rate of hydrogel encapsulation; this is because the CS can be a potent drug encapsulation. ¹⁴ When the ratio of CS to PVA and GNP reaches 2:1:1, the drug loading capacity is the highest, which is due to the fact that CS and PVA can form a three-dimensional mesh structure, which can be loaded with a large number of drugs. ¹⁵ GNP and GEL can enhance the stability of the hydrogel mesh

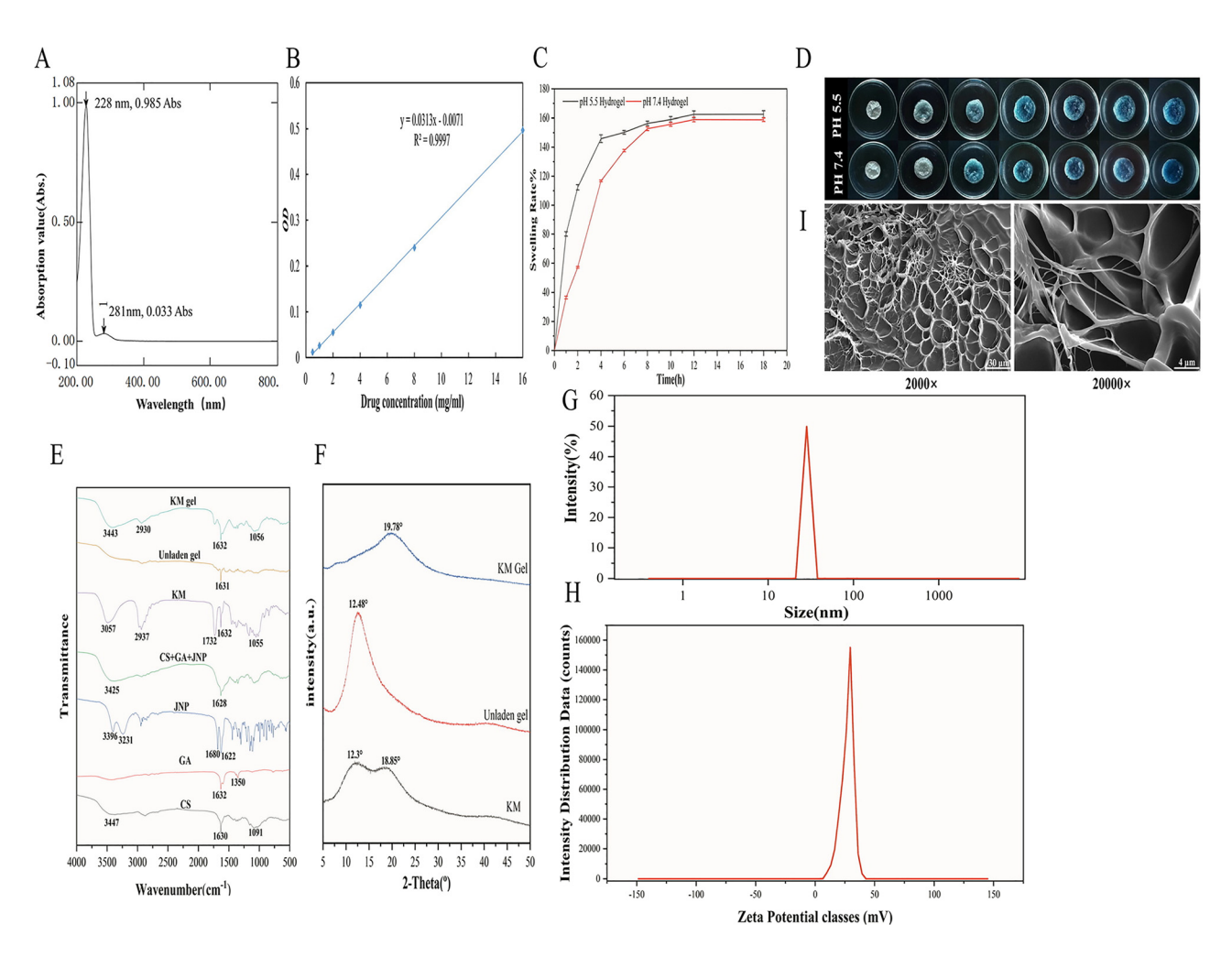


Figure 2: Preparation and characterization of KM hydrogel gels. (A) KM maximum absorption wavelength. (B) KM standard curve. (C) KM hydrogel swelling curve. (D) KM hydrogel swelling picture. (E) FTIR spectrum of KM hydrogel. (F) XRD of MH composite temperature-sensitive gel. (G) Particle size of KM hydrogel. (H) Zeta potential of KM hydrogel. (I) Scanning electron microscope image of KM hydrogel.

Table 1: Results of orthogonal tests.

Level			Factor			EE (%)	LC (%)
	GEL (g)	CS (g)	PVA (g)	GNP (g)	KM (g)		
1	0.2	0.2	0.1	1	0.25	65.2	9.8
2	0.2	0.3	0.2	2	0.25	74.2	10.4
3	0.2	0.4	0.3	3	0.25	81.8	12.7
4	0.3	0.3	0.3	3	0.25	74.8	10.7
5	0.3	0.4	0.2	2	0.25	83.1	13.6
6	0.3	0.2	0.1	1	0.25	66.3	9.4
7	0.4	0.4	0.2	1	0.25	82.6	12.4
8	0.4	0.3	0.3	3	0.25	73.7	9.6
9	0.4	0.2	0.1	2	0.25	65.8	10.3

CS, chitosan; EE, encapsulation rate; GEL, gelatin; GNP, genipin; KM, kitasamycin; LC, loading capacity; PVA; polyvinyl alcohol.

structure, which is due to the fact that GNP is a natural and nontoxic cross-linking agent, can react with amino groups in macromolecular compounds to form a three-dimensional reticular scaffold structure, and the cross-linking products are similar to the cross-linking strength of chemical cross-linking agents, 16 CS chitin is a class of natural aminopolysaccharides derived from more than 55 % of N-acetyl groups, ¹⁷ and GEL is a straight-chain polymer formed by cross-linking amino acids with peptides. 18 GNP can cross-link with amino groups of CS and gelatin via Schiff base to form a stable, three-dimensional reticulated hydrogel.¹⁹

3.2 Evaluation of hydrogel characterization

3.2.1 Swelling property test

The swelling test for hydrogels evaluates their ability to absorb and release pharmaceuticals in slow-release delivery systems. Slow swelling prolongs release and vice versa. Therefore, the swelling behavior is the most important application parameter that determines the prepared hydrogel.²⁰ From Figure 2C and D, it can be seen that the swelling performance of the prepared hydrogel can reach up to 12 h, and the swelling equilibrium is reached after 18 h. The swelling rate of the hydrogel is higher in pH 5.5 than in pH 7.4, which is due to the fact that in acidic condition, many hydrogen bonds are formed between -COOH groups, which narrows their three-dimensional network structure and decreases the swelling rate of the microspheres, and more water can be adsorbed into the three-dimensional network of hydrogels, which increases their swelling rate.²¹ While – COOH was ionized to -COO when the hydrogels were under pH 7.4,²² the swelling rate of hydrogels under alkaline conditions eventually approached that of acidic conditions at

18 h with increasing swelling time, due to the increase in intermolecular electrostatic repulsion. Hydrogel swelling is crucial for wound healing because it regulates medication release but also contributes to the degree of hydrogel adhesion to the wound and exudate absorption, as well as maintaining the optimal moisture for wound healing, thereby accelerating complete epithelialization of the wound.

3.2.2 Particle size and zeta potential

For drug delivery system, most parts of the body can be reached through the microcirculation of capillaries or the pores of various surface membranes. An important requirement for any delivery system is that it has the ability to move freely in a variety of channels. The ability to cross a variety of barriers, and the narrowest capillary has a crosssectional area of 2,000 nm, in fact, to carry out effective delivery, the prepared drug formulations and delivery system should be less than 300 nm in diameter. 23 The hydrogel had an average particle size of 28.56 ± 0.83 nm, allowing for drug delivery via tissue interstitial spaces, thus, exerting the therapeutic effect of the drug. The zeta potential was used to evaluate the stability of the hydrogel. The hydrogel's zeta potential was (16.33 \pm 0.95) mV as reported in the literature, and the prepared hydrogel was relatively stable.

3.2.3 SEM analysis

Porous hydrogels are permeable to both water vapor and wound exudate. The permeability of the wound exudate avoids bulging.²⁴ Figure 2I shows that the hydrogel has an excellent three-dimensional network structure. Furthermore, the CS/Gel/PVA hydrogel has numerous micropores that are evenly dispersed across its surface.

3.2.4 FT-IR analysis

As shown in Figure 2E, the FTIR spectrum of CS has a peak at 1,630 cm⁻¹ corresponding to C=O. The FTIR spectrum of pure gelatin shows a peak at 1,632 cm⁻¹ corresponding to C=O and a bending peak at 1,350 cm⁻¹ corresponding to N-H. The FTIR spectrum of GNP shows a characteristic broad band at 3.450 cm⁻¹ corresponding to N-H. The FTIR spectrum of GNP shows a peak at 1,622 cm⁻¹ corresponding to C=O. The FTIR spectrum of GNP shows a peak at 1,622 cm⁻¹ corresponding to C=O and a characteristic broad band at 3,450 cm⁻¹ corresponding to the O-H stretching vibration of the hydroxyl group of GNP. The FTIR spectra of CS/GEL/GNP hydrogels show two characteristic bands at 3,425 cm⁻¹ and 1,628 cm⁻¹. This suggests that the three materials are formed by Schiff base reaction between amine and aldehyde groups.²⁵ The broad peak of KM at 3,057 cm⁻¹ is formed by the overlapping of O-H and N-H stretching vibrational absorption peaks. The broad peak at 1.632 cm⁻¹ is formed by the overlapping of single bonded C=O with characteristic peak, 2.937 cm⁻¹ C-H stretching vibrational absorption peaks, the broad peak at 1,055 cm⁻¹ is a characteristic peak formed by the overlapping of bending vibrational absorption peaks. The broad peak at 1,631 cm⁻¹ of the unloaded hydrogel is a characteristic peak at single bonded C=O. The characteristic peaks of the prepared KM hydrogel overlapped with those of the KM and unloaded hydrogels, indicating that the KM was encapsulated in the unloaded hydrogel.

3.2.5 XRD analysis

X-ray diffraction was used to assess the physical state (amorphous or crystalline) of the samples.²⁶ Figure 2F compares the diffractograms of the drug (KM) and the prepared hydrogels. The characteristic peaks of KM in the X-ray diffractograms indicate that the drug is in a crystalline form and that the blank and drug-loaded formulations are in a crystalline state. In addition, the diffraction peaks of the loaded formulation formed by combining the drug with the blank formulation were almost identical to that of the drug, suggesting that the drug may have been loaded into the network structure formed by the hydrogel.

3.3 Hydrogel in vitro release rate assay

In current clinical applications, KM has poor water solubility and slightly lower blood concentrations than other macrolide antibiotics,²⁷ so it must be administered in sufficient amounts and frequently to achieve therapeutic goals. Therefore, in vitro drug release devices have gained popularity due to their noninvasiveness, convenient, and prolonged administration. As shown in Figure 3C, in the simulated in vitro release process, the KM solution reaches the release equilibrium after 10 h, while the loaded KM hydrogel still releases the drug after 48 h. The drug is released from the KM solution at 10 h, while the loaded KM hydrogel releases the drug at 48 h. The loading and release of the drug depends on the swelling property of the hydrogel, and it was mentioned that slow swelling could prolong the release time in the hydrogel swelling property test of this study, and the results showed that the slow swelling was observed in pH 7.4, and the in vitro release results verified that the release rate of KM was higher in pH 7.4 than that in pH 5.5. The results proved that the construction of the hydrogel system could prolong the drug action time, thus

improving the disadvantages of low blood concentration of the drug and frequent administration.

3.4 Antibacterial activity of hydrogel

3.4.1 MIC determination

One of the agents selected for this test for S. aureus is the macrolide antibiotic KM. Its special feature is its sensitivity to penicillin G and erythromycin-resistant S. aureus.²⁸ According to Matsumak, of 416 S. aureus strains isolated from the clinic, up to 72 % were resistant to penicillin G, but these strains were sensitive to KM.²⁹ The antimicrobial properties of KM-loaded hydrogels were tested using S. aureus ATCC29213 with SCVA. The MIC value of the solution of KM with KM water against S. aureus ATCC29213 and SCVA was 0.5 µg/mL, as shown by the micro broth dilution method.

3.4.2 Bacteriostatic effect test by agar perforation method

The bacteriostatic effect test by Figure 3A and B can be seen in the drug content of 1 %, 0.10 %, and 0.01 %; KM hydrogel and the same concentration of KM solution inhibition of the size of the circle is basically equal, indicating that the inhibition of this preparation compared with the KM solution is not significantly different.

3.4.3 In vitro bacteriostatic curve plotting

From Figure 3D and E, it can be seen that at the same drug concentration, the difference between the bacteriostatic effect of loaded KM hydrogel and KM solution was not significant, and it was also found that the bacteriostatic time of loaded KM hydrogel was significantly prolonged by 8 h compared to that of KM solution at its measured MIC, and the bacteriostatic time of loaded KM hydrogel was significantly prolonged by 6 h compared to that of KM solution at 1/2 MIC, indicating that the bacteriostatic performance of loaded KM hydrogel has a good effect of controlled drug release.

3.5 Hydrogel safety studies

3.5.1 Blood compatibility testing

The hemolysis rate of loaded KM hydrogel on rabbit erythrocytes is shown in Figure 4A, the erythrocytes were all sunk, and the hemolysis was determined by using the enzyme labeling instrument, which indicated that the loaded

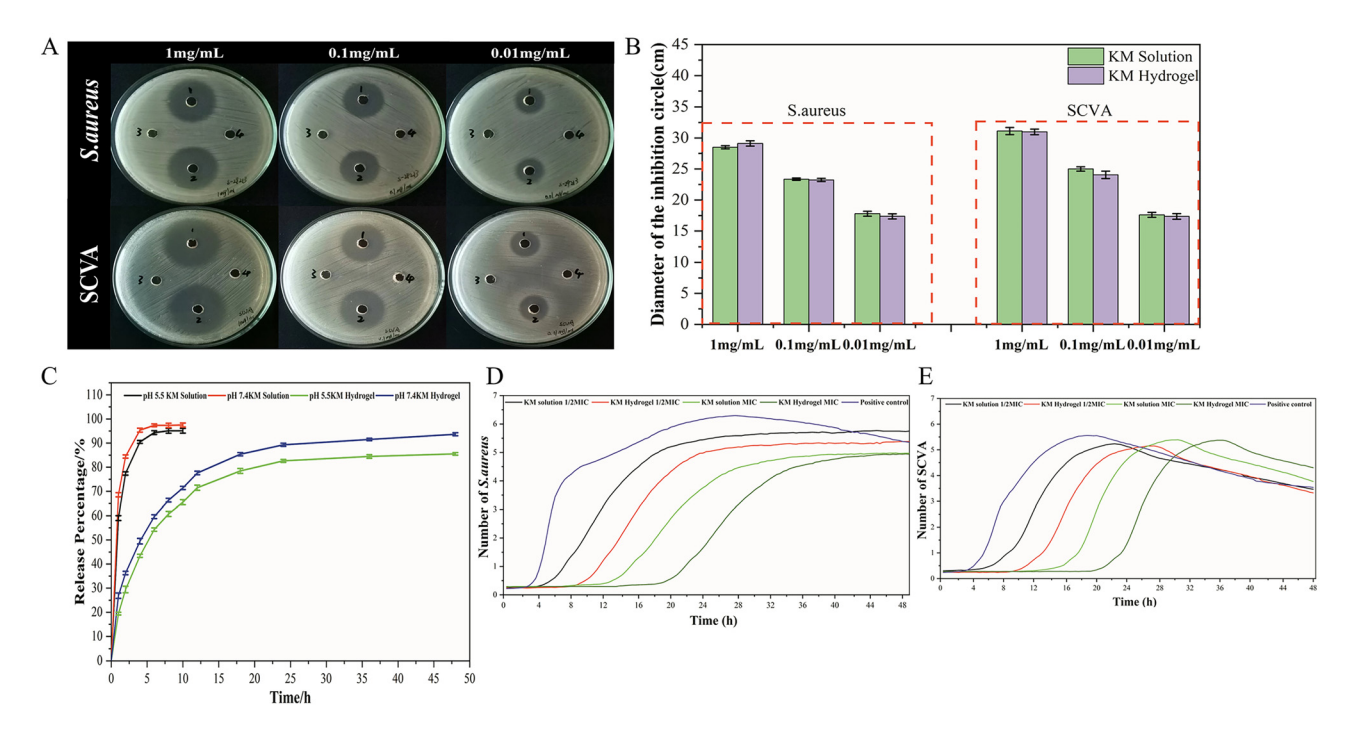


Figure 3: Release rate and antibacterial activity of KM hydrogels *in vitro*. (A) Circle of inhibition of KM hydrogel gels with different concentrations of KM solution (1, KM hydrogel; 2, KM solution; 3, blank hydrogel; 4, blank control). (B) Statistics of the diameter of the inhibition circles (data are mean \pm SD, n = 3). (C) Release profiles of KM hydrogel versus KM solution in PBS at pH 5.5 and 7.4 (n = 3). All data are expressed as mean \pm SD. Statistical significance was calculated by one-way ANOVA (*P < 0.05, **P < 0.01). (D) Inhibition curves of KM hydrogel and KM solution against *Staphylococcus aureus*. (E) Inhibition curves of KM hydrogel and KM solution against SCVA.

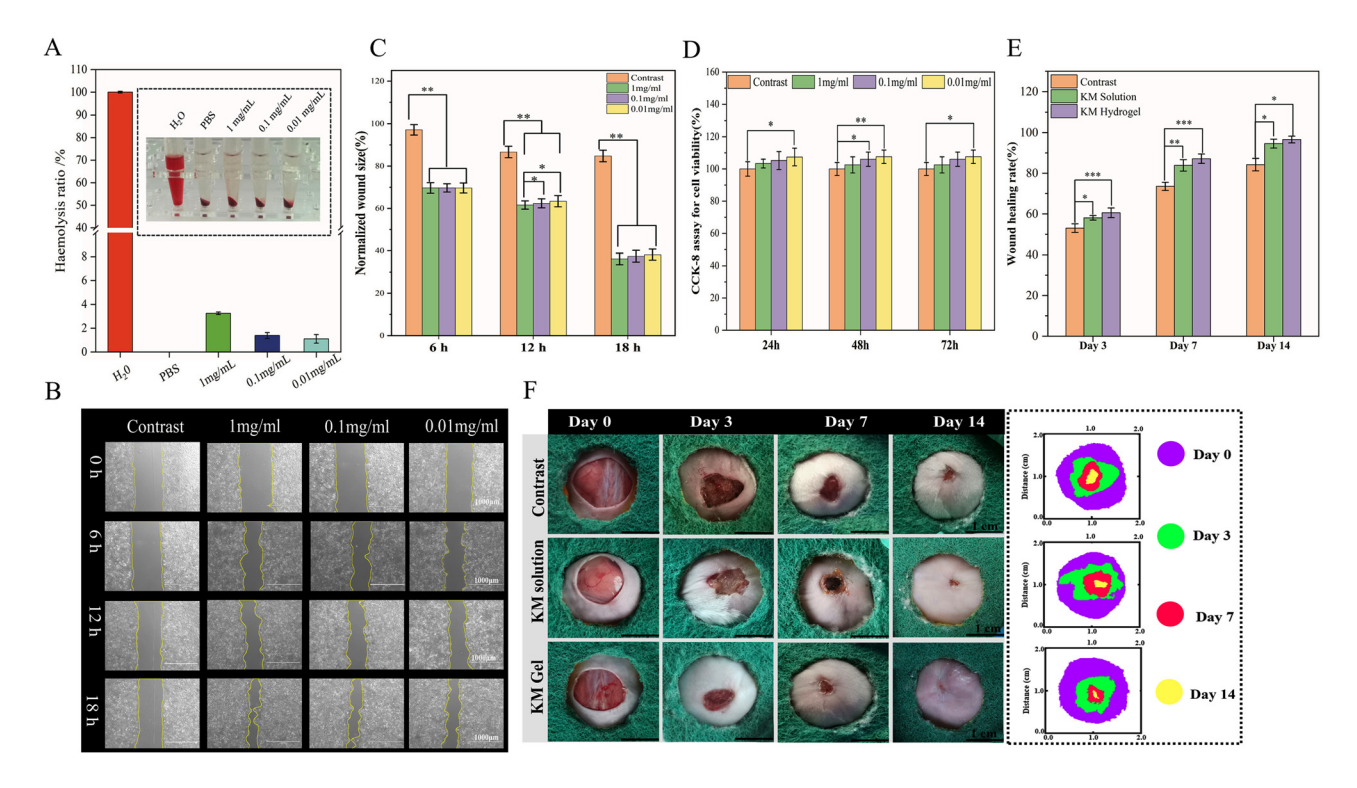


Figure 4: Biocompatibility of KM hydrogel with repair of infected wounds. (A) Effect of KM hydrogel on the hemolysis rate of erythrocytes after 12 h of coincubation with erythrocytes (*n* = 3). (B) Photographs of the scratch area of MAC-T cells at 6, 12, and 18 h with different concentrations of KM hydrogel. (C) Scratch area statistics (*n* = 3). (D) Effect of KM hydrogel on MAC-T cell viability at 24, 48, and 72 h (*n* = 6). (E) Trauma healing rate statistics (*n* = 3). (F) Representative photographs of wounds of different groups at different times (scale bar 1 cm) with trajectories of wound healing (scale bar 1 cm).

KM hydrogel had a very low destructive effect on the erythrocytes and showed excellent blood compatibility in the hemolysis experiment.

3.5.2 Cytotoxicity assay

As shown in Figure 4D, after the MAC-T cells were coincubated with loaded KM hydrogel for 24 h, the cell number of the 0.01 mg/mL group differed from that of the control group (p < 0.05), the proliferation rate of the cells of all groups was higher than 90 %, and the lower the concentration of loaded KM hydrogel, the higher the proliferation between the groups of different concentrations of loaded KM hydrogel. The short time of coincubation may not be able to show the toxic effect of the material on the cells, so in the loaded KM hydrogel and cell coincubation to 48 h and 72 h, we also detected the cell proliferation rate, and the results showed that even for a long time of coincubation up to 72 h, the growth rate of cells in the groups of different concentrations of loaded KM hydrogel was significantly different from that in the control group (24 h, p < 0.01), (72 h, p < 0.05), confirming the excellent cytocompatibility of the loaded KM hydrogels.

3.5.3 Cell migration experiment

Image I software was used to circle the scratched area at different time points, and the scratched area was calculated (Figure 4B and C). The results of the 12 h scratching experiment showed that the scratched area residual rate of the loaded KM hydrogel (1 mg/mL) group was $61.616 \% \pm 1.932 \%$, (0.1 mg/mL) group was $62.373 \% \pm 2.138 \%$, and (0.01 mg/mL)group was $63.383\% \pm 2.636\%$. There was a statistically significant difference between the 3 groups loaded with KM hydrogel compared to the control group $86.650 \% \pm 2.718 \%$ (p < 0.01). Observed to the end point at 18 h, the residual rate of scratch area in the loaded guillamycin hydrogel (1 mg/mL) group was 36.197 % ± 2.722 %, (0.1 mg/mL) group was $37.459\% \pm 2.722\%$, and (0.01 mg/mL) group $38.211\% \pm 2.564\%$, which was still statistically different from that of the control group 84.763 % \pm 2.722 % (p < 0.01), suggesting that loading of KM hydrogel could significantly enhance the migration ability of MAC T cells.

3.6 Assessment of body surface wound healing

The mice in the loaded KM hydrogel group, the KM solution group, and their control group were observed and photographed at the time of wound healing on days 0, 3, 7, and 14. The wound sizes of the three groups of mice at different time

points were then counted and their skin defect healing analyzed (Figure 4E and F). When compared, it was found that in the first 3 days of damage repair, the skin damage repair rates of mice in the loaded KM hydrogel group, KM solution group, and their control group were $60.550 \% \pm 2.347 \%$, $58.0723\% \pm 1.133\%$, and $53.017\% \pm 2.114\%$, respectively, with significant differences in the control group compared to the loaded formulation group (p < 0.01), and the difference was significant compared to the solution (p < 0.05). At 7 days, the skin repair rate of mice in the control group $(73.544\% \pm 2.012\%)$ was significantly different (p < 0.05) and was significantly different (p < 0.001) from that of mice in the KM-loaded hydrogel group (87.149 % \pm 2.308 %), and the difference was significant (p < 0.05) from that of mice in the KM solution group (83.872 $\% \pm 2.82 \%$). At 14 days, the area of healed skin in mice in the KM-loaded hydrogel group increased to 96.599 % \pm 1.661 % of the total defect area in the loaded KM hydrogel group and 94.591 % ± 2.200 % in the KM solution group. At this time, the repair rate in the control group of mice was 84.217 % \pm 3.071 %, which was significantly different from that in the loaded formulation group compared to the mice in the solution group (p < 0.05). This is attributed to a number of reasons, one of which is that hydrogels are three-dimensional structures that provide optimal moisture, mimic the skin, and act as a barrier to invading microorganisms, and also CS in hydrogel substrates has been used as a wound healing enhancer. The main biochemical roles of CS in wound healing are fibroblast activation, cytokine production, macrophage migration, and stimulation of type IV collagen synthesis.³⁰

3.7 Histopathologic examination

The quality of the freshly produced skin was evaluated through the application of histological analysis. H&E staining was used to visualize the integrity of the newly formed skin attachments, dermis, and epidermis. The black line with two arrows in Figure 5A illustrates the granulation tissue fiber thickness, and the boundary between the dermis and epidermis is shown by a yellow dotted line. Additional quantitative evaluation in comparison to the control combination KM solution group (Figure 5E) demonstrated that the thickness of the wound skin tissue in the loaded KM hydrogel group increased the fastest and that the wound healing process showed a faster re-epithelialization process.

Collagen is a major component of the extracellular matrix and plays an important role in the function of skin tissues.³¹ The Masson staining results are shown in Figure 5C and F. Compared with the amount of collagen deposited at 14 days postoperatively, the total amount of collagen deposited at the wound site on the seventh day of wound

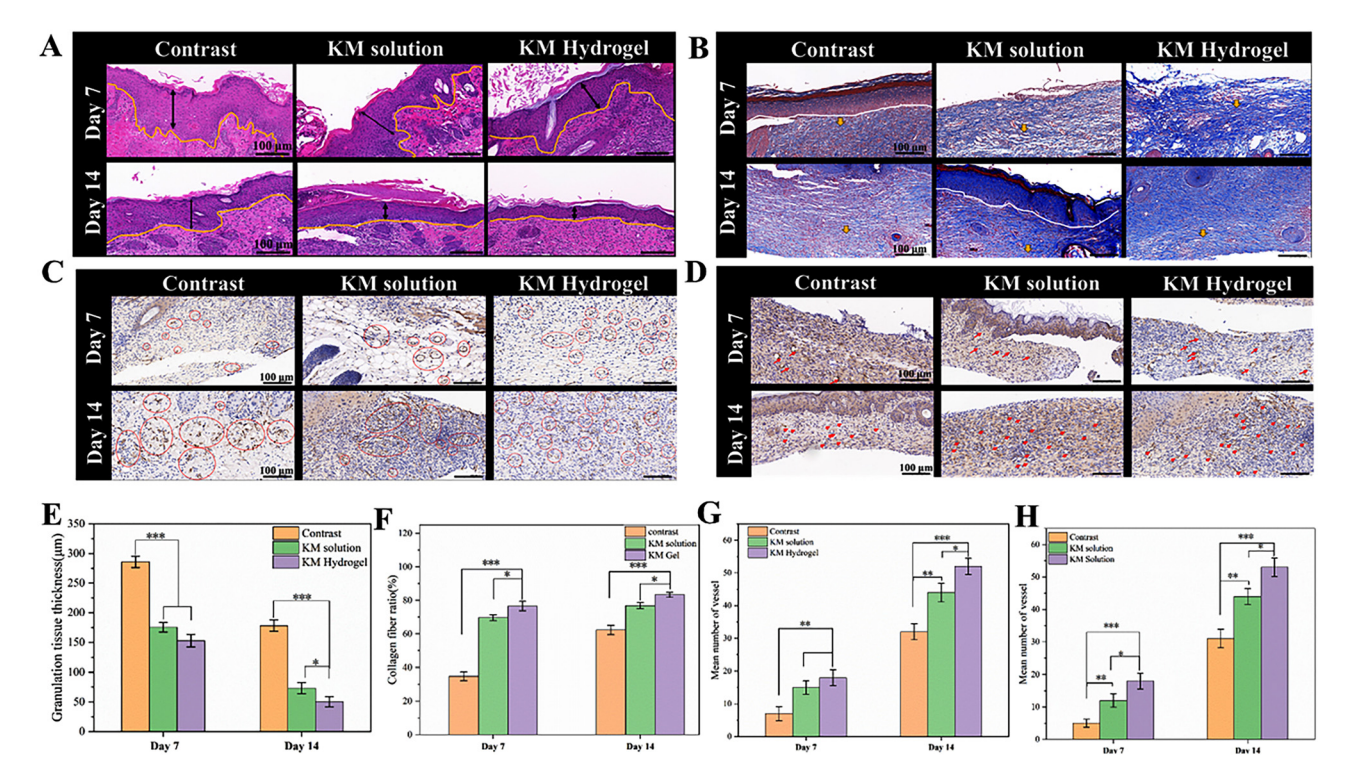


Figure 5: Histological analysis of the wound healing process. (A) Representative HE staining results of trauma tissue after days 7 and 14 of treatment (scale bar 100 µm, black double arrows indicate granulation tissue; yellow line indicates epidermal and dermal junction). (B) Granulation tissue measurements using slide viewer (n = 3). (C) Representative Masson staining of traumatized tissue after days 7 and 14 of treatment (collagen fibers in blue, scale bar 100 µm). (D) Quantification of the area covered by collagen fibers using image J (n = 3, yellow arrows indicate collagen fibers; white line indicates epidermal-dermal junction). (E) IHC staining results of representative CD31 of trauma tissue after days 7 and 14 of treatment (scale bar 100 µm, red circles indicate the number of neo vessels). (F) Number of neo vessels counted using slide viewer (n = 3). (G) IHC staining of representative VEGF in trauma tissue after treatment days 7 and 14 (scale bar is 100 µm, red arrows indicate the number of neo vessels). (H) Neovascularization counts using slide viewer (n = 3).

healing was relatively less. It appeared to be a lighter blue color in the Masson staining plots. The reason for this is that at 7 days postop, the wound is still mainly in the inflammatory response stage and relatively few fibroblasts infiltrate the wound site; at 14 days postop, wound healing is in the proliferation and remodeling stage, when the number of fibroblasts increases and the synthesis and deposition of collagen is significantly enhanced, thus appearing as a darker blue color in Masson's staining plots. Taken together, the overall trends at 7 and 14 days postoperatively remained consistent, i.e., more collagen was able to be deposited in the wound site treated with loaded KM hydrogel compared to the control group, the KM solution group, and the loaded KM hydrogel group.

3.8 Expression of CD31 and VEGF during wound healing

CD31 is a platelet-endothelial cell adhesion factor commonly used in immunohistochemistry to characterize endothelial

cell organization and assess angiogenesis. 32 Immunohistochemical analysis of CD31 was performed to characterize the degree of neovascularization in skin wound sections from the seventh day after hand surgery, and the results are shown in Figure 5B-G. The number of blood vessels was richer in the KM solution group and the loaded KM hydrogel group, especially in the loaded KM hydrogel group, where a greater number of thick blood vessels with a more disorganized structural arrangement were seen, which was notably greater than what the control group experienced. VEGF, or vascular endothelial growth factor, is a major growth factor that promotes wound repair and is highly specific for vascular endothelial cells. Activating its receptor can induce vascular endothelial cell migration and proliferation. Secondly, VEGF also promotes the migration of keratinocytes and fibroblasts.³³ Immunohistochemical analysis of VEGF was performed on skin wound sections on day 7 after hand surgery and the results are shown in Figure 5D-H. The loaded KM hydrogel group had the highest positive rate and richest VEGF content compared to the control and KM solution groups.

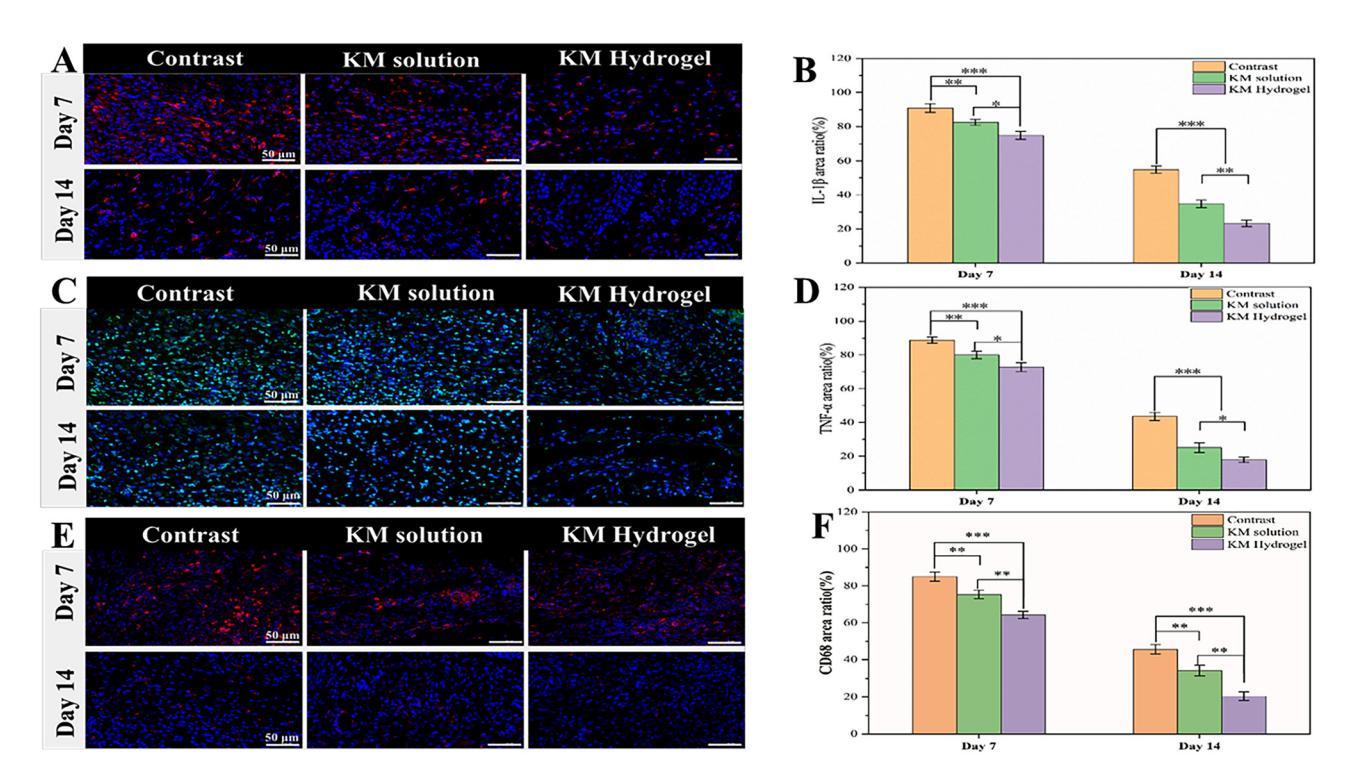


Figure 6: Expression of associated factors. (A) Representative IL-1 β if staining results of traumatized tissue after days 7 and 14 of treatment (IL-1 β red, scale bar 50 μm). (B) Quantitative analysis of IL-1 β coverage area using image J (control data defined as 100 %, n = 3). (C) Representative TNF- α if staining of trauma tissue after days 7 and 14 of treatment (TNF- α green, scale bar 50 μm). (D) Quantitative analysis of TNF- α coverage area using Image J (control data defined as 100 %, n = 3). (E) Representative CD68 staining of trauma tissue after days 7 and 14 of treatment (CD68 red color, scale bar 50 μm). (F) Quantitative analysis of CD68 coverage area using Image J (control data defined as 100 %, n = 3). All data are expressed as mean \pm SD. Statistical significance was calculated by one-way ANOVA (*P < 0.05, **P < 0.01, ***P < 0.001).

3.9 Expression of IL-1 β , TNF- α , and CD68 during wound healing

The inflammatory phase is the first period of wound healing, and IL-1 β and TNF- α are typical proinflammatory cytokines closely associated with the inflammatory response in the early stages of healing.³⁴ Immunofluorescence of two factors, IL-1 β and TNF- α , was used to evaluate the efficacy of the loaded KM hydrogel during the inflammatory period. As shown in the figure, both IL-1 β and TNF- α levels at the wound site were significantly lower in the loaded KM hydrogel group compared to the control, KM solution, and loaded KM hydrogel groups at both 7 and 14 days postoperatively (Figure 6A and B). Figure 6C and D present the quantitative analysis of IL-1 β and TNF- α content, respectively, and as shown by the area ratio, the IL-1\beta and TNF- α content of the loaded KM hydrogel could be reduced to approximately 20% of the control group at 14 days postoperatively. All of these findings on the inflammatory response point to the ability of the KM-loaded hydrogel to lessen inflammation at the wound site and improve the conditions for wound healing.

Using the macrophage antibody CD68 for immunofluorescence staining of the tissue, the early inflammatory response was further evaluated. As shown in Figure 6E and F, red fluorescence-labeled macrophages were visible at the hydrogel-tissue interface on day 7 of treatment. However, by postoperative day 14, almost no macrophages were visible, demonstrating the good histocompatibility of the loaded KM hydrogel. In addition, macrophages polarize into proinflammatory M1-type cells and prodamage repair M2-type cells. Polarized macrophages release cytokines, extracellular enzymes, and other inflammatory mediators that affect other cellular functions in the inflammatory milieu. Therefore, rational control of macrophage responses also facilitates trauma repair.

There are several explanations for the remarkable role of loaded KM hydrogels in promoting wound healing. First, the high hydrophilicity of CS allows the hydrogel to retain wound moisture, which promotes cell adhesion and migration, leading to faster skin regeneration and preventing scab formation. GEL, as a product of collagen hydrolysis, not only acquires the original biocompatibility, biodegradability, and low immunogenicity of collagen but also exposes the

Arg-Gly-Asp (RGD) sequence and matrix metalloproteinase (MMP) targeting sequence sites,³⁶ which can be further recognized by integrin receptors on the cell membrane surface, facilitating cell adhesion and proliferation. The outcomes verify that the loaded KM hydrogel possesses possible uses as a slow-release medication delivery system and to aid wound healing.

4 Conclusions

Hydrogels were prepared using CS, GEL, and PVA as hydrogel matrix and KM as test drug; they showed good swelling rate and antimicrobial activity. Fourier transform infrared (FTIR) spectroscopy verified the compatibility of KM with the hydrogel, and XRD analysis confirmed the stable crystalline nature of the hydrogel. Scanning electron microscopy analysis showed that the hydrogel had a threedimensional reticulated pore structure. Animal experiments clearly demonstrated that the use of hydrogel as a KM delivery system helped to shorten wound healing time and promote wound healing. Histopathological evaluation also confirmed this observation. It was demonstrated that the findings could be used for controlled drug release and to promote skin wound healing.

Acknowledgments: The authors would like to thank Tarim University, China, for providing research equipment and experimental materials. The authors acknowledge the assistance of Instrumental Analysis Center of Tarim University.

Research ethics: All the animal experiments were performed following the guideline approved by the Institution Animal Care and Use Committee (IACUC) at the Animal Research Ethics Committee of Tarim University (2023024), Xingjiang, China. The authors affirm that the current research study does not involve human subjects.

Author contributions: Bei Ma: conceptualization, methodology, software, investigation, formal analysis, writing original draft. Junfeng Liu and Hongwei Chen: conceptualization, funding acquisition, resources, supervision, writing review & editing. Lijun Tang: data curation, formal analysis. Ze Ding and Tianyang Wang: writing – review & editing. Pan Liu and Yaofeng Zhang: investigation, data curation. Tianzhen Dong and Zhengyang Zhao: writing – review & editing. The authors certify that this paper has not been published or submitted for publication elsewhere at the same time and in its all form has been read and approved by all authors.

Competing interests: The authors affirm that they have no relevant financial or nonfinancial interests to disclose.

Research funding: This work was supported by the Engineering Laboratory of Tarim Animal Diseases Diagnosis and Control, Xinjiang Production & Construction Group (grant no. ELDC202401); the Engineering Laboratory of Tarim Animal Diseases Diagnosis and Control, Xinjiang Production & Construction Group (grant no. ELDC202201).

Data availability: The authors affirm that the datasets generated and analyzed during the current study are available from the corresponding author, Junfeng Liu, on reasonable request.

References

- 1. Kamoun, E. A.; Kenawy, E. R. S.; Chen, X. A Review on Polymeric Hydrogel Membranes for Wound Dressing Applications: PVA-Based Hydrogel Dressings. J. Adv. Res. 2017, 8 (3), 217-233.
- 2. Pourshahrestani, S.; Zeimaran, E.; Kadri, N. A.; Mutlu, N.; Boccaccini, A. R. Polymeric Hydrogel Systems as Emerging Biomaterial Platforms to Enable Hemostasis and Wound Healing. Adv. Healthc. Mater. 2020, 9 (20), 2000905.
- 3. Ye, L.; Zhang, Y.; Wang, Q.; Zhou, X.; Yang, B.; Ji, F.; Dong, D.; Gao, L.; Cui, Y.; Yao, F. Physical Cross-Linking Starch-Based Zwitterionic Hydrogel Exhibiting Excellent Biocompatibility, Protein Resistance, and Biodegradability. ACS Appl. Mater. Interfaces 2016, 8 (24), 15710-15723.
- 4. Wang, H.; Xu, Z.; Zhao, M.; Liu, G.; Wu, J. Advances of Hydrogel Dressings in Diabetic Wounds. Biomater. Sci. 2021, 9 (5). 1530-1546.
- 5. Wang, S.; Wei, Y.; Wang, Y.; Cheng, Y. Cyclodextrin Regulated Natural Polysaccharide Hydrogels for Biomedical Applications: a Review. Carbohydr. Polym. 2023, 313, 120760.
- 6. Stout, E. I.; McKessor, A. Glycerin-Based Hydrogel for Infection Control. Adv. Wound Care 2012, 1 (1), 48-51.
- 7. Qin, W.; Long, S.; Panunzio, M.; Biondi, S. Schiff Bases: A Short Survey on an Evergreen Chemistry Tool. Molecules 2013, 18 (10), 12264-12289.
- 8. Yang, H.; Li, X.; Wang, Y.; Wang, G. Progress in the Study of the Resistance of Staphylococcus aureus to Macrolides and the Mechanism of Resistance. Livest. Vet. Med. 2015, 47 (12), 141-144.
- 9. Zhang, X. Analysis Of Drug Resistance of Staphylococcus aureus in Dairy Cow Mastitis and Isolation, Identification and Application of Phages; Shandong Agricultural University, 2022.
- 10. Zhou, X. C.; Duan, W. Y.; Zeng, S. The Efficacy of Kithamycin Combined with High-Dose Vitamin C in the Treatment of Pediatric Mycoplasma Pneumonia. Matern Child Health Care China 2017, 32 (19), 4724–4727.
- 11. Zhan, Q. D.; Wang, Q. N.; Yu, D. G. Study on the In Vitro Antibacterial Effect of Domestically Produced Crystalline Leucomycin. Antibiotics 1987 (5), 356-360.
- 12. Li, M. Pharmacology and Clinical Applications of Guillamycin. J. Chin. Pharm. 1993 (9), 524-526.
- 13. National Pharmacopoeia Commission Pharmacopoeia of the People's Republic of China: Part II; China Medical Press: Beijing, 2020.
- 14. Meyer-Déru, L.; David, G.; Auvergne, R. Chitosan Chemistry Review for Living Organisms Encapsulation. Carbohydr. Polym. 2022, 295, 119877.
- 15. Han, Y.; Xu, Y.; Tian, L.; Zhou, J.; Zhou, X. [Research Progress of Polyvinyl Alcohol (PVA) Based on Hydrogel Dressings]. Zhongguo Yi Liao Qi Xie Za Zhi 2018, 42 (6), 437-439.

- 16. Yu, Y.; Xu, S.; Li, S.; Pan, H. Genipin-cross-linked Hydrogels Based on Biomaterials for Drug Delivery: A Review. Biomater. Sci. 2021, 9 (5), 1583-1597.
- 17. Ibrahim, M. A.; Alhalafi, M. H.; Emam, E. A. M.; Ibrahim, H.; Mosaad, R. M. A Review of Chitosan and Chitosan Nanofiber: Preparation, Characterization, and its Potential Applications. Polymers 2023, 15 (13), 2820.
- 18. Andreazza, R.; Morales, A.; Pieniz, S.; Labidi, J. Gelatin-Based Hydrogels: Potential Biomaterials for Remediation. Polymers 2023, 15 (4), 1026.
- 19. Chiono, V.; Pulieri, E.; Vozzi, G.; Ciardelli, G.; Ahluwalia, A.; Giusti, P. Genipin-crosslinked Chitosan/Gelatin Blends for Biomedical Applications. J. Mater. Sci. Mater. Med. 2008, 19 (2), 889-898.
- 20. Wang, T.; Zhang, F.; Zhao, R.; Wang, C.; Hu, K.; Sun, Y.; Politis, C.; Shavandi, A.; Nie, L. Polyvinyl Alcohol/Sodium Alginate Hydrogels Incorporated with Silver Nanoclusters via Green Tea Extract for Antibacterial Applications. Des. Monomers Polym. 2020, 23 (1), 118-133.
- 21. Shi, Y.; Zheng, T.; Shang, Q. Preparation of Acrylic/Acrylate Copolymeric Surfactants by Emulsion Polymerization Used in Pesticide Oil-In-Water Emulsions. J. Appl. Polym. Sci. 2012, 123 (5), 3117-3127.
- 22. Spagnol, C.; Rodrigues, F. H. A.; Pereira, A. G. B.; Fajardo, A. R.; Rubira, A. F.; Muniz, E. C. Superabsorbent Hydrogel Composite Made of Cellulose Nanofibrils and Chitosan-Graft-Poly(Acrylic Acid). Carbohydr. Polym. 2012, 87 (3), 2038-2045.
- 23. Ram, B. G.; Uday, B. K. Nanoparticle Technology for Drug Delivery: Boca Raton, 2006.
- 24. Hinrichs, W. L. J.; Lommen, E. J. C. M. P.; Wildevuur, C. R. H.; Feijen, J. Fabrication and Characterization of an Asymmetric Polyurethane Membrane for Use as a Wound Dressing. J. Appl. Biomater. 1992, 3 (4),
- 25. Hu, K.; Jia, E.; Zhang, Q.; Zheng, W.; Sun, R.; Qian, M.; Tan, Y.; Hu, W. Injectable Carboxymethyl Chitosan-Genipin Hydrogels Encapsulating Tea Tree Oil for Wound Healing. Carbohydr. Polym. 2023, 301, 120348.
- 26. Rojek, B.; Gazda, M.; Plenis, A. FTIR, Raman Spectroscopy and HT-XRD in Compatibility Study between Naproxen and Excipients. Spectrochim. Acta Part A: Mol. Biomol. Spectrosc. 2023, 302, 123048.
- 27. Gong, X.; Hou, C.; Zhang, Q.; Li, Y.; Wang, H. Thermochromic Hydrogel-Functionalized Textiles for Synchronous Visual Monitoring of On-Demand In Vitro Drug Release. ACS Appl. Mater. Interfaces 2020, 12 (46), 51225-51235.

- 28. Matsumae, A.; Onuma, M. Leucomycin Sensitivity Bacteria Isolated from Patients. J. Antibiot. 1958, 11 (3), 104-108.
- 29. Sezer, A. D.; Hatipoglu, F.; Cevher, E.; Oğurtan, Z.; Bas, A. L.; Akbuğa, J. Chitosan Film Containing Fucoidan as a Wound Dressing for Dermal Burn Healing: Preparation and In Vitro/In Vivo Evaluation. AAPS PharmSciTech 2007, 8 (2), E94-E101.
- 30. Feng, Z.; Zhang, Y.; Yang, C.; Liu, X.; Huangfu, Y.; Zhang, C.; Huang, P.; Dong, A.; Liu, J.; Liu, J.; Kong, D.; Wang, W. Bioinspired and Inflammation-Modulatory Glycopeptide Hydrogels for Radiation-Induced Chronic Skin Injury Repair. Adv. Healthc. Mater. 2023, 12 (1),
- 31. Zha, S.; Utomo, Y. K. S.; Yang, L.; Liang, G.; Liu, W. Mechanic-Driven Biodegradable Polyglycolic Acid/Silk Fibroin Nanofibrous Scaffolds Containing Deferoxamine Accelerate Diabetic Wound Healing. Pharmaceutics 2022, 14 (3), 601.
- 32. Sun, G.; Zhang, X.; Shen, Y. I.; Sebastian, R.; Dickinson, L. E.; Fox-Talbot, K.; Reinblatt, M.; Steenbergen, C.; Harmon, J. W.; Gerecht, S. Dextran Hydrogel Scaffolds Enhance Angiogenic Responses and Promote Complete Skin Regeneration during Burn Wound Healing. Proc. Natl. Acad. Sci. U. S. A. 2011, 108 (52), 20976-20981.
- 33. Qu, J.; Zhao, X.; Liang, Y.; Zhang, T.; Ma, P. X.; Guo, B. Antibacterial Adhesive Injectable Hydrogels with Rapid Self-Healing, Extensibility and Compressibility as Wound Dressing for Joints Skin Wound Healing. Biomaterials 2018, 183, 185-199.
- Kreimendahl, F.; Marquardt, Y.; Apel, C.; Bartneck, M.; Zwadlo-Klarwasser, G.; Hepp, J.; Jockenhoevel, S.; Baron, J. M. Macrophages Significantly Enhance Wound Healing in a Vascularized Skin Model. J. Biomed. Mater. Res. A 2019, 107 (6), 1340-1350.
- 35. Chen, H.; Xing, X.; Tan, H.; Jia, Y.; Zhou, T.; Chen, Y.; Ling, Z.; Hu, X. Covalently Antibacterial Alginate-Chitosan Hydrogel Dressing Integrated Gelatin Microspheres Containing Tetracycline Hydrochloride for Wound Healing. Mater. Sci. Eng.: C. 2017, 70, 287–295.
- Babavalian, H.; Latifi, A. M.; Shokrgozar, M. A.; Bonakdar, S.; Mohammadi, S.; Moosazadeh Moghaddam, M. Analysis of Healing Effect of Alginate Sulfate Hydrogel Dressing Containing Antimicrobial Peptide on Wound Infection Caused by Methicillin-Resistant Staphylococcus aureus. Jundishapur J. Microbiol. 2015, 8 (9), e28320.